doi:10.1093/brain/awp222 Brain 2009: 132; 3047–3059 | 3047

BRAIN
A JOURNAL OF NEUROLOGY

Spatial characterization of interictal high frequency oscillations in epileptic neocortex

Catherine A. Schevon,[1] A. J. Trevelyan,[2] C. E. Schroeder,[3] R. R. Goodman,[4] G. McKhann Jr[4] and R. G. Emerson[1,5]

1 Department of Neurology, Columbia University, New York, NY, USA
2 School of Neurology, Neurobiology and Psychiatry, University of Newcastle, Newcastle Upon Tyne, UK
3 Department of Psychiatry, Columbia University, New York, NY, USA
4 Department of Neurological Surgery, Columbia University, New York, NY, USA
5 Department of Pediatrics, Columbia University, New York, NY, USA

Correspondence to: Catherine A. Schevon,
Neurological Institute,
710 West, 168th Street,
NY 10032,
USA
E-mail: cas2044@columbia.edu

Interictal high frequency oscillations (HFOs), in particular those with frequency components in excess of 200 Hz, have been proposed as important biomarkers of epileptic cortex as well as the genesis of seizures. We investigated the spatial extent, classification and distribution of HFOs using a dense $4 \times 4\,mm^2$ two dimensional microelectrode array implanted in the neocortex of four patients undergoing epilepsy surgery. The majority (97%) of oscillations detected included fast ripples and were concentrated in relatively few recording sites. While most HFOs were limited to single channels, ~10% occurred on a larger spatial scale with simultaneous but morphologically distinct detections in multiple channels. Eighty per cent of these large-scale events were associated with interictal epileptiform discharges. We propose that large-scale HFOs, rather than the more frequent highly focal events, are the substrates of the HFOs detected by clinical depth electrodes. This feature was prominent in three patients but rarely seen in only one patient recorded outside epileptogenic cortex. Additionally, we found that HFOs were commonly associated with widespread interictal epileptiform discharges but not with locally generated 'micro-discharges'. Our observations raise the possibility that, rather than being initiators of epileptiform activity, fast ripples may be markers of a secondary local response.

Keywords: multichannel extracellular recording; epilepsy; intracranial EEG; interictal epileptiform activity; fast ripples; high frequency oscillations

Abbreviations: HFOE = high frequency oscillation event; HFOs = high frequency oscillations; iEEG = intracranial electroencephalography; MEA = microelectrode array; MUA = multiunit activity; NREM = non-rapid eye movement; μEEG = Electroencephalography derived from microelectrode recording

Introduction

High frequency oscillations (HFOs), or brief events in the high gamma band (>80 Hz), have been proposed as useful biomarkers of epileptic pathology. It has been suggested that fast ripples, or population bursts oscillating at rates >200 Hz, may be largely restricted to the epileptogenic zone in temporal lobe epilepsy (Bragin *et al*., 1999; Staba *et al*., 2002; Jirsch *et al*., 2006; Urrestarazu *et al*., 2007; Worrell *et al*., 2008) and in neocortical epilepsy syndromes (Jacobs *et al*., 2008). Studies in rodent

Received May 4, 2009. Revised June 12, 2009. Accepted July 11, 2009. Advance Access publication September 10, 2009

epilepsy models have indicated that fast ripples or population bursts oscillating at rates higher than 200 Hz are present interictally in epileptic rats (Bragin *et al*., 2003) and play important roles during epileptogenesis (Bragin *et al*., 2000, 2002, 2007) and at seizure onset (Bikson *et al*., 2003; Bragin *et al*., 2005). On the other hand, evoked oscillations in the fast ripple range have been found in recordings from the somatosensory cortex of normal rats (Gibson *et al*., 1999) and humans (Haueisen *et al*., 2001). This suggests that, like the lower frequency (<200 Hz) ripple oscillations found in normal rodent hippocampus (Buzsaki *et al*., 1992) and normal primate thalamus and neocortex (Schroeder *et al*., 1992, 1995; Steinschneider *et al*., 1992), fast ripples may also play a role in normal neocortical processing. Thus, further characterization of fast ripples and particularly of differences between fast ripples recorded from epileptogenic versus non-epileptogenic cortex, will be helpful if fast ripples are to be used to delineate epileptogenic areas for the purposes of epilepsy surgical treatment.

A concern underlying the study of fast ripples is that they are highly restricted both spatially and temporally (Bragin *et al*., 2003) and thus may not be sampled adequately in macroelectrode or sparse microcontact recordings. While fast ripples have been detected with depth macroelectrodes (Jirsch *et al*., 2006; Urrestarazu *et al*., 2007), comparison of simultaneous recordings from macroelectrodes and microwire bundles (Worrell *et al*., 2008) found clear differences in detection rates and frequency distributions. The limited spatial sampling of microcontacts may help to isolate spatially restricted events such as fast ripples; it could, however, adversely affect detection if the events are sparsely distributed.

The discovery of 'microdischarges' and 'microseizures' in microelectrode recordings from epileptogenic neocortex provide additional evidence of very fine-scale architecture of epileptiform activity (Schevon *et al*., 2008). However, the precise relationship of these microscale features to interictal epileptiform events typically recognized in subdural macroelectrode recordings and to fast ripples remains to be determined.

To address these questions, we evaluated interictal HFOs recorded from a dense two dimensional microelectrode array (MEA) ($4 \times 4\,mm^2$, 0.4 mm spacing) implanted in epilepsy patients undergoing chronic invasive monitoring. Microelectrode or microwire recordings in epilepsy patients have previously been used to acquire otherwise unobtainable information on the neurophysiology of both epilepsy (Bragin *et al*., 1999; Staba *et al*., 2002; Ulbert *et al*., 2004*a, b*; Worrell *et al*., 2008) and normal cognition (Wang *et al*., 2005; Cash *et al*., 2009). In this report, we investigate the spatial extent and fine-scale distribution of neocortical ripples and fast ripples, and characterize their relationship to disturbances of electrocerebral activity detected by both the MEA and subdural macroelectrodes.

Materials and methods

Microelectrode array implantation

The MEA used in this study is an FDA-approved device (Neuroport™ neural monitoring system, Cyberkinetics Neurotechnology Systems, Foxboro, MA) that has been safely implanted in humans at several institutions (Hochberg *et al*., 2006; House *et al*., 2006; Waziri *et al*., 2009). The array measured $4 \times 4\,mm^2$ and contained 96 microelectrodes arranged in a regular 10×10 square with no electrodes at the corner positions. The individual microelectrodes were platinum-coated silicon, protruding 1 mm from the array base and were electrically insulated except for the terminal 70 μm. They tapered from 35 to 75 μm in diameter at the base to 3–5 μm at their recording tips. Electrode impedance at manufacture was 322 ± 138 kOhm.

The MEA was implanted alongside subdural and depth electrodes into the neocortex of patients with medically intractable focal epilepsy undergoing intracranial electroencephalography (iEEG) recording at the Columbia University Medical Center and the New York-Presbyterian Hospital to help to identify the epileptogenic zone, i.e. the tissue that must be removed to obtain seizure control (Rosenow and Luders, 2001). Use of the MEA was limited to patients for whom the presurgical evaluation indicated clear seizure localization to a restricted region and in whom invasive recording was performed to refine the resection boundaries, in order to ensure that the implantation site was included in the area targeted for subsequent surgical treatment. Cases that were considered appropriate included temporal lobe epilepsy, in which implantation was performed to define the contribution of lateral temporal neocortex and tailor temporal lobectomy, and extratemporal syndromes in which scalp EEG recording indicated a consistent and well-defined interictal and ictal focus limited to a sublobar distribution and confirmed by a neuroimaging study. The study was approved by the Institutional Review Board of the Columbia University Medical Center and informed consent was obtained from each patient prior to the procedure.

The MEA was implanted into flat surfaces of exposed neocortical gyri through the pia mater using a pneumatic insertion technique (for more details, see Suner *et al*., 2005; Hochberg *et al*., 2006; Waziri *et al*., 2009). The implant site was selected based on the estimation of the epileptogenic region from pre-surgical studies, as described above, and selected so as to be included in the subsequent surgical treatment. Lateral temporal sites were chosen to fall within the region to be included in anterolateral temporal lobectomy. Extratemporal implantation sites were selected from regions with prominent interictal epileptiform discharges identified by intraoperative corticography, a standard clinical procedure during subdural electrode implantation at our institution. Potentially eloquent sites such as Broca's area or primary motor cortex were avoided. Following implantation, standard clinical macroelectrode grids were placed. The MEA assembly includes two reference wires: one was placed subdurally near the MEA and the other epidurally. During monitoring, MEA data were made available to the clinical team to assist in the surgical evaluation. Following the monitoring period, with duration determined by clinical needs, the MEA was explanted along with the clinical grids. Gross pathology and histopathology of the implant sites were evaluated. These studies revealed no gross tissue damage, minimal tissue injury with microscopic haemorrhages and microglial activation localized to the electrode insertion sites, and little evidence of neuronal death. These findings are similar to those reported in animal histopathology studies (Rousche and Normann, 1998). Neuronal degeneration at the microelectrode sites was minimal and far less marked than that associated with clinical depth electrode implantation, which is considered to be a safe procedure. These results are being reported separately.

The epileptogenic zone was determined by the consensus of at least two epileptologists at the Columbia Comprehensive Epilepsy Center, based on interictal and ictal intracranial and scalp video-EEG, neuroimaging studies and results of functional evaluation. The location of the MEA relative to both the cortical surface and the subdural

macroelectrodes was identified by intraoperative photographs and frameless stereotactic localization (Brainlab, Westchester, IL), combined with postoperative imaging studies.

Dual modality recording

MEA signals were sampled at 30 kHz/channel (0.3–7.5 kHz bandpass filtering) with 16-bit precision and a range of ±8 mV. The reference signal was selected to optimize recording quality; most often it was found that best results were obtained using the pedestal ground as the reference. To monitor recording integrity, electrode impedance testing and visual inspection of sample data was performed after the initial hook-up and daily thereafter.

iEEG was recorded from standard clinical electrodes (Ad-tech Medical Instrument Corp., Racine, WI or PMT Corp., Chanhassen, MN), 4.0 or 4.5 mm diameter platinum disks spaced 1 cm centre to centre and arranged in a grid or strip. Data were acquired at 500 Hz/channel with 24-bit precision (0.5–125 Hz bandpass filtering) using a standard clinical video-EEG system (XLTek Inc., Oakville, ON, Canada). Two contacts of an epidurally placed electrode strip, with electrodes facing away from the dura, served as the reference. Coded sequences of transistor–transistor logic pulses delivered simultaneously to digital inputs of both acquisition systems were used to align iEEG and MEA recordings.

Microdischarge and macrodischarge detection

Offline, MEA recorded data were down-sampled to 500 Hz/channel after low pass filtering at 125 Hz (fourth order Butterworth) to yield high spatial resolution local field potential signals in the frequency range of standard EEG ('μEEG'). Synchronized μEEG and iEEG data were then converted into identical digital formats, merged into combined files and viewed in spatially organized, referential montages using a commercial EEG viewing program (Insight, Persyst Development Corp., Prescott, AZ).

Each patient's recording was reviewed visually in its entirety by two neurophysiologists (C.A.S. and R.E.) to identify interictal discharge populations and seizures. In the case of differing interpretations, a joint review was conducted and the more conservative interpretation was agreed upon. Wake and non-rapid eye movement (NREM) sleep periods were determined by identifying periods of increased iEEG theta and delta activity combined with simultaneous video evidence. μEEG features likely to represent interictal and ictal epileptiform abnormalities were identified visually and classified based on the waveform characteristics analogous to well-recognized epileptiform abnormalities in standard resolution electroencephalography (Niedermeyer and Lopes da Silva, 1999), as well as correlation to simultaneous iEEG events. Interictal epileptiform events seen in nearby iEEG channels and occurring simultaneously over a broad distribution in the low-pass filtered μEEG are referred to as 'macrodischarges'. Conversely, spatially restricted waveforms seen only in the μEEG with an epileptiform appearance were identified as 'microdischarges' (Schevon *et al*., 2008). An example of a typical microdischarge, associated with a fast ripple oscillation, is shown in Fig. 1b. The rates of each discharge type were determined by visually inspecting the first 5 min of the recording samples analysed for HFOs (described below). Additionally, the MEA channels at which microdischarge activity was present at any time during both recording samples were identified for each patient.

High frequency oscillation detection and classification

HFOs in MEA recorded data were determined by combining the automatic detection technique described by Staba *et al*. (2002) with visual screening by two neurophysiologists (C.A.S. and R.E.). Automated detection was performed using bipolar signals, obtained by pairing orthogonally adjacent channels, to avoid possible contamination by referential artifact; visual screening was then performed separately on each channel.

Two 30 min recording samples for each patient, one during waking and one during NREM sleep, were chosen from the interictal recording. Samples were required to be at least 4 h before or after a seizure, at least 48 h after surgery to minimize the effects of anaesthesia, and free of transient artefacts detected either visually or by inspecting 100–500 Hz time-frequency plots. After bandpass filtering between 100–500 Hz (90th order finite impulse response), the automated detection algorithm was applied. The algorithm, as originally defined, applies the following criteria to epochs of at least 6 ms in duration: (i) root mean square amplitude of at least 5 SD above the mean for the rectified signal over the recording sample being tested; and (ii) at least six peaks with amplitude >3 SD above the mean. This method has a reported sensitivity of 84% compared with manual review (Staba *et al*., 2002). For the purpose of this study, the sensitivity of the automatic detection algorithm was increased by reducing the number of signal peaks required from six to four. The detected samples were then reviewed visually to achieve 100% specificity.

Visual review and event classification were carried out using a custom-developed display that simultaneously shows views of the HFO along with the surrounding μEEG channels (Matlab, Mathworks Inc., Natick, MA) (Fig. 1). The detected event was displayed in four separate frequency bands, derived by symmetrically bandpass filtering the raw data (90th order FIR): μEEG, ripples (80–200 Hz), fast ripples (200–500 Hz), and multiunit activity (MUA). The latter was conservatively defined to be from 800 Hz to 3 kHz to avoid overlap with the fast ripple band, and was displayed as a rectified signal. Simultaneously, a 5×5 subregion of the MEA over a 4 s time slice centred on the start time and at the location of the detected HFO was shown, to permit distinguishing micro- from macrodischarges. Reviewers recorded the time span of each HFO and classified them visually by HFO type, correlation with multiunit spikes, and correlation with μEEG features. Ripples were defined as HFOs that were visible in the ripple band but not in the fast ripple band, while fast ripples were defined as HFOs that were visible in the 200–500 Hz band, with or without visible activity in the ripple band. HFOs were classified according to their temporal association with microdischarges, whether in the same channel or a neighbouring channel, and with macrodischarges.

Spatial distribution of high frequency oscillations

The MEA recorded a large number of channels in regularly spaced locations from a tiny cortical region, providing opportunity for determining the spatial extent and occurrence pattern of HFOs. To study patterns of simultaneous detections, we introduce the term 'HFO event' (HFOE) to signify the detection of one or more HFOs in different channels during time intervals that were either overlapping or at most 6 ms apart. An HFOE can therefore consist of either one or several individual HFO detections and involve one or more channels. To estimate the size of the cortical region spanned

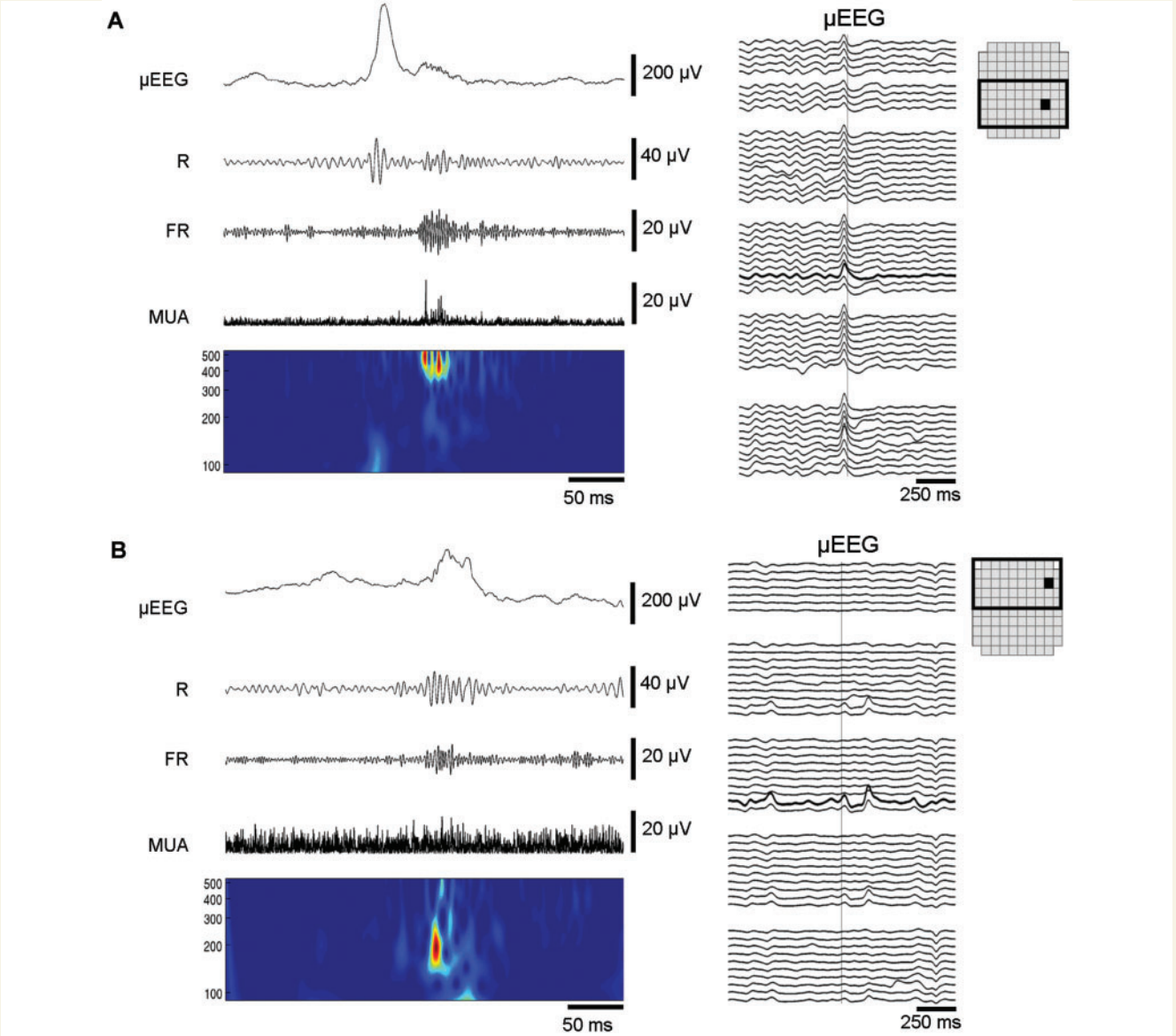

Figure 1 Ripples, fast ripples and their μEEG correlates. (**A**) Fast ripple correlating with a macrodischarge. Left panel: Data from a 350 ms time slice filtered to produce four views: μEEG with high frequencies preserved (2–500 Hz), ripple (R) (100–200 Hz), fast ripple (FR) (200–500 Hz), and MUA (800 Hz to 3 kHz). Below is a time-frequency plot (100–500 Hz) computed using the Morlet wavelet transform. Right panel: Two seconds of 2–50 Hz μEEG from the surrounding MEA channels (enclosed box in the MEA schematic), organized by row (top to bottom) and column (channel groups, left to right). The HFO channel is indicated by the heavy black trace; with the detection at the vertical grey line. Note the timing of the fast ripple after the μEEG discharge peak. The increase in MUA amplitude coincides with the fast ripple but not the preceding ripple oscillation or the discharge peak. This timing pattern of the fast ripple, MUA and discharge peak was typical of many macrodischarge-associated HFO detections. (**B**) Ripple with peak frequency at 200 Hz correlating with a microdischarge. In contrast to the macrodischarge shown in (**A**), the field of the μEEG waveform (right panel) is limited. The relative prominence of ripple activity and the occurrence of the HFO with the discharge peak were typical of HFOs associated with microdischarges.

by the HFO detections within a single HFOE, we determined the area of the smallest square enclosing the detection sites in units of channels, i.e. the number of channels covered by the square. Simultaneous detections occurring in two adjacent channels could be either due to a larger area of origin or to a single restricted-area event detected in two nearby channels. The latter cannot, however, be the case if the number of channels is greater than two. Accordingly, we refer to HFOEs spanning an area of more than two channels as 'large-scale'. For example, in Fig. 2a, the area of the HFOE is equal to one, while Fig. 2b depicts a large-scale HFOE with an area of 80 (8×10).

Relative location of high frequency oscillations and microdischarges

To test whether fast ripples and microdischarges are co-located, we calculated Euclidean distance in units of microelectrode spacing from

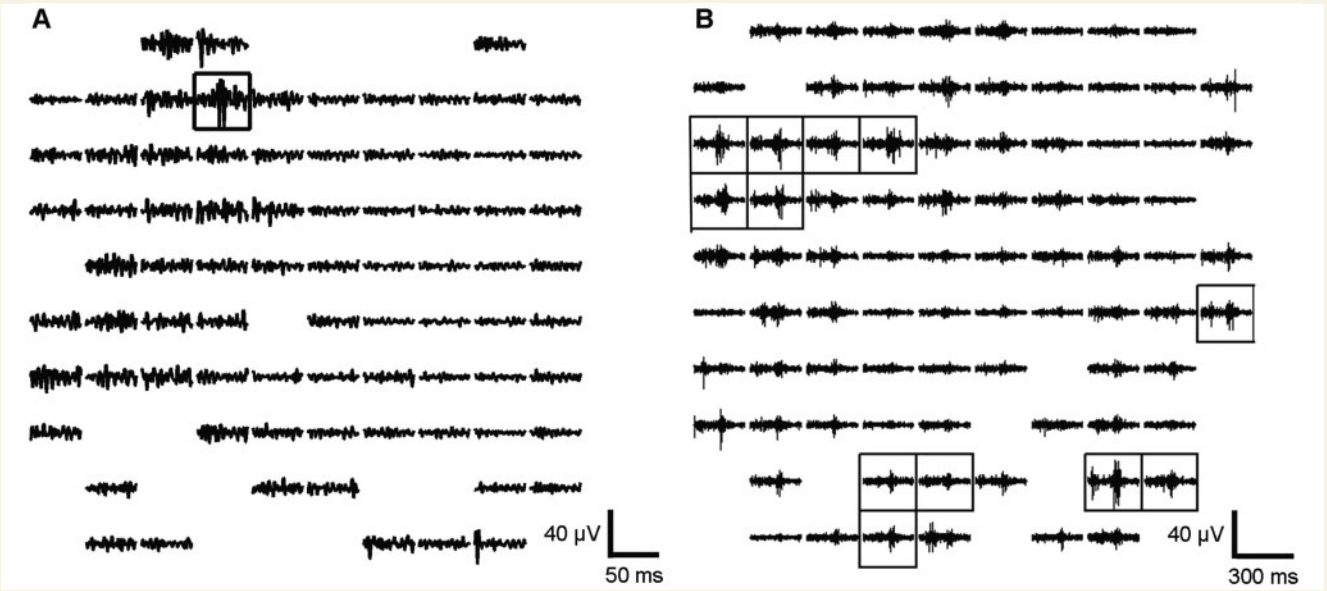

Figure 2 Spatial pattern of high frequency activity during two HFOEs. The MEA is represented according to its physical layout as a 10×10 grid, with each channel corresponding to one square. Within each square, 100–500 Hz bandpass filtered signal is shown. Channels excluded because of data quality and the empty corner positions are indicated by blank squares. Solid black boxes mark channels at which HFOs were detected. (**A**) HFOE with a single HFO detection from Patient 1. The fast ripple shown in the boxed channel is not seen in neighbouring channels, located at orthogonal distances of 400 μm. (**B**) Large-scale HFOE associated with a macrodischarge in Patient 4. The time scale reflects the longer duration of the events depicted. The transient increase in 100–500 Hz activity within the time period shown can be seen in the majority of channels, however, not all these met amplitude or duration criteria relative to baseline for HFO detection (see 'Materials and methods' section). The figure illustrates how the use of objective detection criteria can mask subthreshold increases in high frequency activity. Differences in amplitude and temporal pattern of the waveforms are apparent, even in adjacent channels.

each HFO to the nearest microdischarge site. For example, an HFO detected at a site adjacent to a channel in the same MEA row or column at which microdischarges were recorded was considered to have a distance of one. If HFO activity was always generated from the same sites as those responsible for microdischarges, the distances thus obtained would be zero. Conversely, if HFOs are equally likely to be generated at each MEA channel, the values in the distance vector would be variable and would depend on the distribution of microdischarge sites. To obtain this hypothetical uniform-distribution distance vector, a set of N/R HFO detections at each channel (N = number of HFOs, R = number of recording channels) was assumed and the distances computed as above. Statistically significant differences between the actual and hypothetical distance vectors and the actual and zero distance vectors were then determined using the Wilcoxon signed rank test. Thus, if HFO activity was generated from channels 'neighbouring' microdischarge sites, the expected value of the distance vector would be greater than zero but smaller than it would be if HFOs were uniformly distributed throughout the MEA.

Results

Five patients with medically refractory epilepsy were implanted with the Neuroport device. One patient experienced cyclic seizures every 10–40 min throughout the 48 h monitoring period, so that no definite interictal periods were recorded. This patient was therefore not included in the study. Clinical data for the remaining four patients are summarized in Table 1. Data were recorded from all patients during the entire time they were implanted, for 5–14 days. All had non-lesional epilepsy syndromes originating either from the mesial/basal temporal region (two patients) or the lateral frontal lobe (two patients). The MEA was located within the epileptogenic zone in three patients (Patients 2–4). In Patient 1, the MEA was implanted in lateral temporal neocortex ~4 cm posterior to the anterior temporal pole, a region standardly included in non-dominant anterolateral temporal lobectomy for medically refractory mesial temporal lobe epilepsy, but which did not show independent or propagated epileptiform activity. Subsequent to the recordings, the cortical location of the MEA was resected or treated with multiple subpial transections in each case.

Macrodischarges and microdischarges were only found in the recordings where the MEA was located within the epileptogenic zone (Patients 2–4) (Schevon *et al*., 2008). No microdischarges or macrodischarges were seen in Patient 1's recording. The rates of microdischarges and macrodischarges (Table 2) were highly variable in Patients 2–4, with the number of microdischarge sites ranging from 8 to 24 (mean 15.7) or from 9% to 28% of the total recorded channels (mean 13%). Visual inspection of the aligned iEEG and μEEG recordings revealed that microdischarges did not correlate with disturbances in the activity of nearby macroelectrodes. The macrodischarge correlates in the surrounding

Table 1 Clinical summary

Patient	Implant location	MEA location	Epileptogenic zone	Pathology
1 (41F)	Right lateral and subtemporal regions	Right middle temporal gyrus 4 cm from anterior temporal pole	Right mesial temporal lobe	Non-specific, no mesial temporal sclerosis (MTS), no dysplasia
2 (30M)	Left lateral frontal, mesial frontal, and lateral temporal lobes	Left lateral frontal, minimum distance 2 cm superior to Broca's area and on different gyrus	Boundaries not defined but maximal area identified in left superior/lateral frontal lobe	N/A (MST only)
3 (39M)	Left lateral and mesial frontal lobe	Left lateral frontal, minimum distance 1.5 cm superior to Broca's area and on different gyrus	Left frontal operculum ($3 \times 3\ cm^2$ cortical area), superior to Broca's area	Non-specific
4 (25F)	Left lateral and subtemporal regions	Left inferior temporal gyrus 2.5 cm from anterior temporal pole	Left mesial and anterolateral temporal lobe	Mild MTS

Summary of clinical data for the four patients, including demographic information, pathology results, the location covered by the clinical implant and the location of the MEA in each case. In the case of Patient 3, the MEA was located within the maximally involved area in the left frontal lobe, however the clinicians elected to perform multiple subpial transection (MST) instead of a resection because an additional epileptogenic region was found in the temporal lobe.

Table 2 Features associated with HFOs

Patient	Sample	Macro-discharge rate/min	Micro-discharge rate/min	Percentage of HFOs associated with μEEG features			Percentage of macro-discharges with HFO	Percentage of micro-discharges with HFO	Percentage of HFOs with increased MUA		Percentage of LS-HFOEs with macro-discharges
				Macro	Micro	ND			R	FR	
1	Wake	0	0	–	–	100	–	–	0	100	–
	Sleep	0	0	–	–	100	–	–	0	100	–
2	Wake	5.2	4.4	62	5	33	81	8	2	97	88
	Sleep	10.5	4.5	63	0	37	51	0	0	90	100
3	Wake	76	48	51	8	41	12	3	0	98	100
	Sleep	52.8	90	33	4	63	11	0.8	1	98	51
4	Wake	9.0	7.0	53	6	41	28	3.4	3	94	100
	Sleep	9.0	3.2	33	5	61	18	3.0	2	82	39
Average				49[a]	5[a]	46[a]	33[a]	3.0[a]	1	95	80[a]

Data are shown for each patient's recording samples (wake and NREM sleep). The percentages of HFOs associated with macrodischarges ('Macro'), associated with microdischarges ('Micro') or occurring in isolation ('ND') are given. As Patient 1's recording contained no macro- or microdischarges at the MEA site, all HFOs are classed as ND, and no percentage calculations pertaining to these μEEG features were performed. The rates of macrodischarge and microdischarge detections in each recording sample are shown, along with the proportions of each discharge type that were associated with HFOs. While significant variation was present, macrodischarges were significantly more likely to be associated with HFOs than microdischarges (Student's *t*-test, $P < 0.05$). Large-scale HFOEs (LS-HFOE) were strongly associated with macrodischarges (40%–100%, mean 79%). Fast ripples were strongly associated with multiunit spiking, while the opposite was true of ripples.
a Averaged from Patients 2–4 only.

macroelectrodes, on the other hand, revealed significant variability in relative timing (Fig. 3) that suggested differing source locations and propagation pathways.

HFOs were detected in both wake and sleep interictal recording samples of all four patients (Fig. 4). The rate of individual HFO detections over all channels (per recording sample) ranged from 2.6 to 22.5/min (mean 10.9), with Patient 1 having the lowest rates. Rates were generally higher in NREM sleep (individual rate 4.6–22.46, mean 11.0) than in waking (2.6–20.4, mean 10.7); however, the difference was not statistically significant. For individual channels at which HFOs were detected, the per-channel average rate varied between 0.03 and 0.24 (mean 0.12) HFOs per minute. The maximum rate for a single channel in a given recording sample, however, was an order of magnitude higher, up to 6.4 HFOs per minute in the wake sample from Patient 3 and averaging 2.3 detections per minute (Fig. 4).

High frequency oscillations classification

HFOs were classified by visual review as either ripples (80–200 Hz) or fast ripples (visible in the 200–500 Hz band), as well as whether the HFO correlated with visible multiunit spiking (Table 2). Oscillations limited to the ripple range were relatively rare and none were found in Patient 1's recording. In contrast, nearly all HFOs either combined ripple and fast ripple components, or were pure fast ripples (86%–100%, mean 97%). The amplitudes of

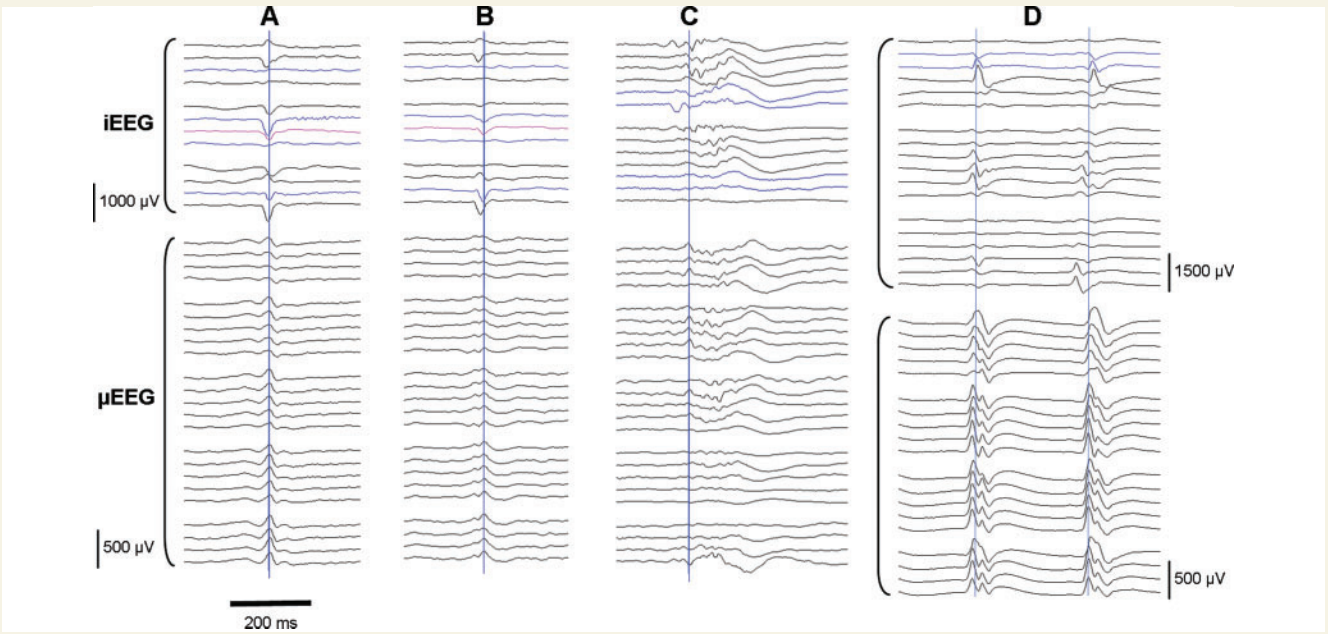

Figure 3 Macrodischarges and their iEEG correlates. Top grouping: recordings from subdural grid macroelectrodes surrounding the MEA are shown, organized by row and column; blue traces indicate macroelectrodes adjacent to the MEA, and pink traces indicate subdural electrodes directly overlying the MEA. Bottom grouping: selected MEA channels (every other channel in each row and column); channels organized by row. Vertical blue lines are provided for convenience in viewing aligned waveform features. (**A** and **B**) Two macrodischarges from Patient 3. The discharge in **A** appears to align closely with the μEEG waveforms, but the discharge in **B** is seen to lead in from the bottom iEEG channel. (**C**) Macrodischarge from Patient 2, with earliest peak appearing in the top row of iEEG channels. (**D**) Macrodischarges from Patient 4, again showing variations in the relative discharge latencies in the iEEG record. These samples suggest that the location of the MEA relative to the discharge source and propagation pathway is variable.

ripple components varied from 10 to 76 μV (mean 21 μV), and the amplitudes of fast ripple components varied between 2 and 26 μV, with a mean of 5 μV. Most strikingly, fast ripples correlated strongly with increased MUA (82%–100%), while ripples rarely had any MUA correlate (0%–3%). Consistent with prior reports (Buzsaki *et al*., 1992; Bragin *et al*., 2007; Foffani *et al*., 2007), populations of unit spikes were seen to coincide with the peaks of fast ripple but not ripple oscillations (Fig. 1).

HFOs were further classified by visual review according to their association with μEEG features (Table 2). Overall, 49% of detections in Patients 2–4 were associated with macrodischarges, ranging from 33% in the sleep recordings of Patients 3 and 4 to 63% in both of Patient 2's recording samples. While prior reports of neocortical interictal epileptiform events associated with HFOs in depth macroelectrode recordings indicate that the high frequency activity often rode the discharge peaks (Jirsch *et al*., 2006; Urrestarazu *et al*., 2007), we found that in our data, fast ripple components were often seen trailing the peaks. HFOs not associated with interictal epileptiform events comprised all of Patient 1's HFO detections and 46% of those recorded from the other three patients. In contrast, there were comparatively few detections associated with microdischarges; on average 5% of detections in Patients 2–4 occurred in conjunction with microdischarges that were seen either in the same channel or an adjacent channel. We also directly measured the proportion of macrodischarges and microdischarges that were associated with HFO activity; while those proportions varied markedly between patients, the difference between macrodischarges (mean 33%) and microdischarges (mean 3%) was clear and significantly different (Student's *t*-test, $P < 0.05$).

Large-scale high frequency oscillation events

We investigated the number and location of channels involved in HFOEs in order to estimate their extent within the $4 \times 4\,mm^2$ boundaries of the MEA. Compared with the rate of single HFO detections (mean 10.9/min), the somewhat lower HFOE rates per minute (Fig. 4; overall range 2.3–18.1, mean 8.3) reflect the multiple contemporaneous HFO detections seen in most recording samples. While most HFOEs involved only a single microelectrode channel, simultaneous HFO detections spanning more than two channel sites were seen in 12% (Fig. 4). Such large-scale HFOEs were rare in Patient 1, while they were significantly more common in the other three patients (Student's *t*-test, $P < 0.05$). These multiple detections were never seen with microdischarges but were commonly associated with macrodischarges (Table 2).

The HFOs comprising large-scale HFOEs revealed a high degree of local variability, as evidenced by variations in waveform morphology, frequency range and timing. Figure 5 shows an example of two channels from a typical large-scale HFOE, illustrating the differences that can occur even over short distances.

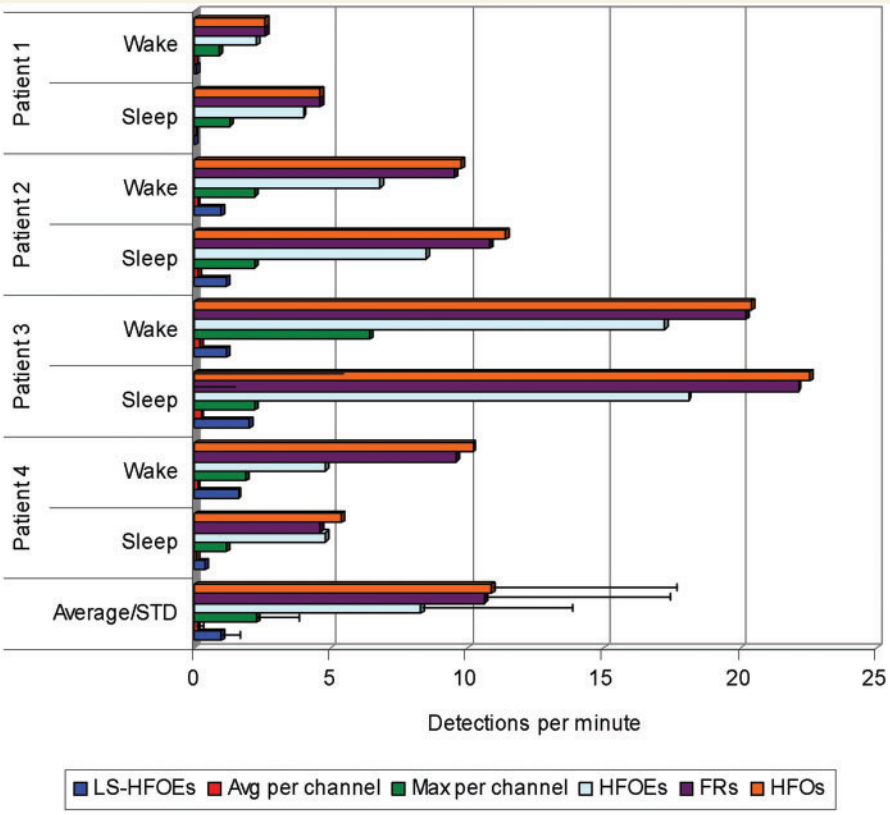

Figure 4 HFO detection rates per minute in wake and NREM sleep samples. The coloured bars depict rates of HFOs, including all single channel detections; HFOEs, which take simultaneous detections into account; fast ripples; the maximum and average HFOs per channel; and large-scale HFOEs, which comprised a minority of HFO detections overall (12%). The average of each measure (bottom set) with standard deviation indicated by error bars are shown across all wake and sleep samples. Because of the large number of channels, the average rate per channel is very small (range 0.03–0.24, mean 0.12). In comparison to Patient 1, Patients 2–4 showed significantly more frequent HFOs and large-scale HFOEs (Student's *t*-test, $P < 0.05$).

Spatial distribution of high frequency oscillations

HFO detections showed a strong tendency to cluster in distinct spatial patterns that were unique to each patient and were relatively consistent across recording samples for the same patient (Fig. 6). Table 3 shows the percentage of channels in each recording sample at which any HFOs were detected, which ranged from 9% in Patient 1 to 30% in Patient 3. In each case, however, a relatively small number of channels were responsible for the majority of HFO detections. The area from which half or more HFO detections occurred covered between 2.3% to 6.3% of recording channels.

Relationship of high frequency oscillation generators to microdischarge sites

Localization of microdischarges and HFOs revealed that, while the two phenomena were distinct from each other, there was a suggestion of a spatial association. Figure 6 shows schematics of the MEA depicting both HFO detection rates by location as well as the sites at which microdischarges were seen at any time in the chronic recording. Clustering of HFOs at a relatively small number of sites is clearly seen, both in the MEA maps and the accompanying histograms of HFO rates per channel. Aside from Patient 1, in whom no microdischarges were recorded, the HFOs appeared to cluster around microdischarge sites. We investigated this further by measuring Euclidean distance between each detected HFO and its nearest microdischarge site and comparing this to the distances computed for a hypothetical uniform distribution of HFO detections (see 'Materials and methods' section). In each of the three patients in whom both microdischarges and HFOs were present, there was a significant difference between the actual and hypothetical measures (Wilcoxon signed rank test, $P < 0.05$), with the mean of the distances of actual HFOs to microdischarge sites being smaller than that calculated for the hypothetical uniform distribution (Table 3).

Discussion

This study utilized a dense, 96-channel two dimensional MEA implanted into epileptic neocortex to resolve the fine spatial

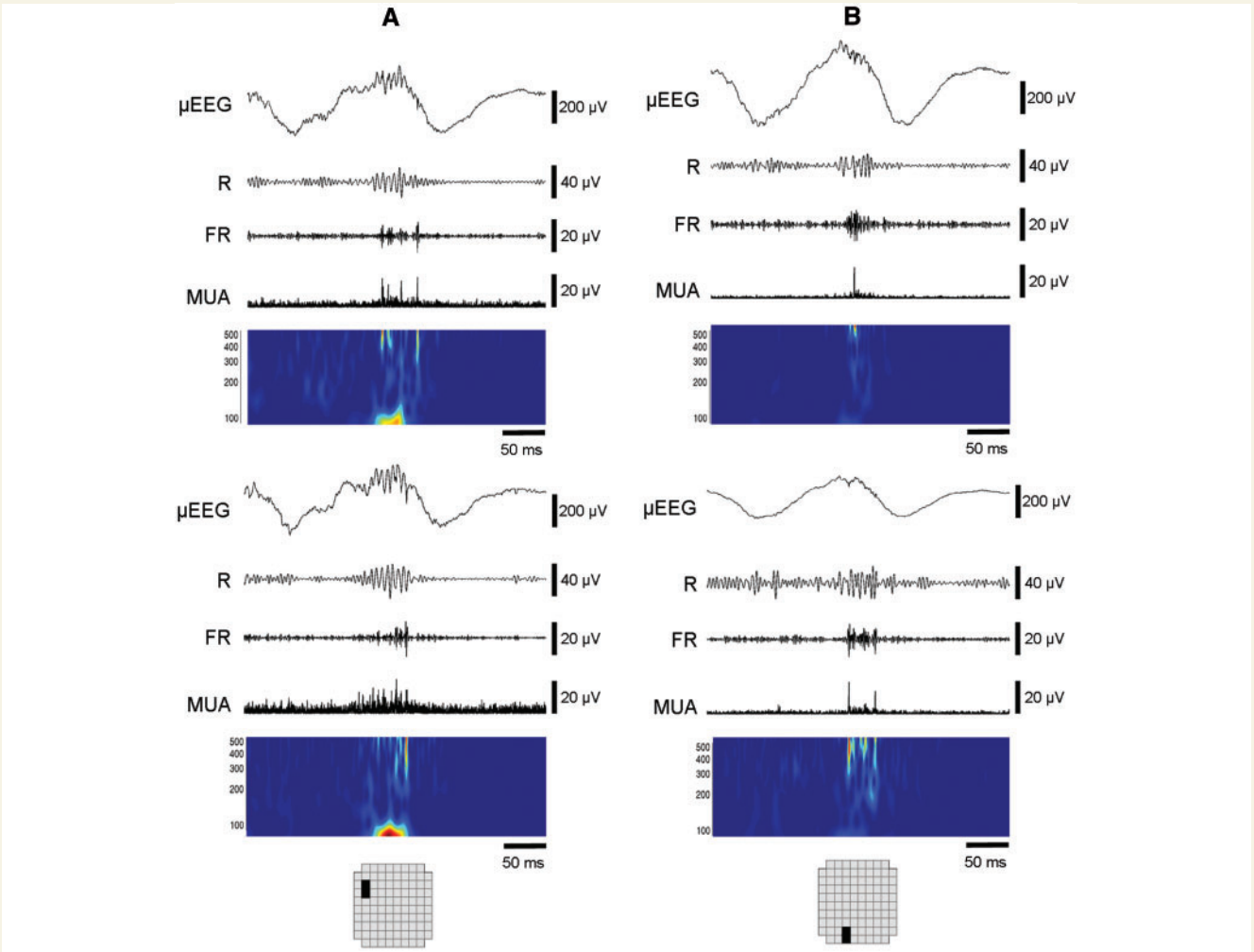

Figure 5 HFOs occurring simultaneously during a macrodischarge recorded from Patient 4. Two pairs of adjacent channels in different areas of the MEA are shown (**A**, **B**; solid black boxes in schematics). The same time slice is shown in all four panels, with signals displayed as in Fig. 1. Note the marked differences in timing, morphology, and frequency range in both the 100–500 Hz bands and in MUA between adjacent recording sites. For example, in (**B**) the maxima of the fast ripple amplitude envelope are clearly seen to occur at different times in the two channels, while in (**A**) there is fast ripple activity in the top channel that is not reflected in the bottom channel. These observations indicate that recording sites separated by 400 μm are capable of distinguishing independent generators of high frequency activity.

structure of interictal HFOs. The HFOs in this data set, almost all of which showed fast ripple components, were both highly localized and concentrated in a small proportion of MEA channels. Detection rates and the extent of the spatial distribution were both significantly greater within the epileptogenic zone. Additionally, we found evidence of large scale simultaneous HFO activation, most often in association with macrodischarges, but with marked differences in the oscillation characteristics between channels; these were rarely seen in the only patient recorded outside the epileptogenic zone. As HFOs only rarely accompanied microdischarges and were found at different sites, it is clear that they are distinct phenomena, albeit with a possible link indicated by their locations relative to each other.

High frequency oscillation occurrence rates and classification

Taking all MEA channels into account, the rate of HFO detections (11/min on average) far exceeds rates reported in studies using implanted microwires, which range from 0.25 (Staba *et al*., 2002) to 3.0/min (Worrell *et al*., 2008). However, the average detection rate *per MEA channel* (0.12 HFOs per minute) is similar to these earlier findings, suggesting that random sampling of a subset of MEA channels would produce results similar to those seen with sparser-sampling microwires. The high detection rate then is most likely an effect of the dense spatial sampling afforded by the MEA's 400 μm inter-electrode spacing, combined with the finding that HFOs are

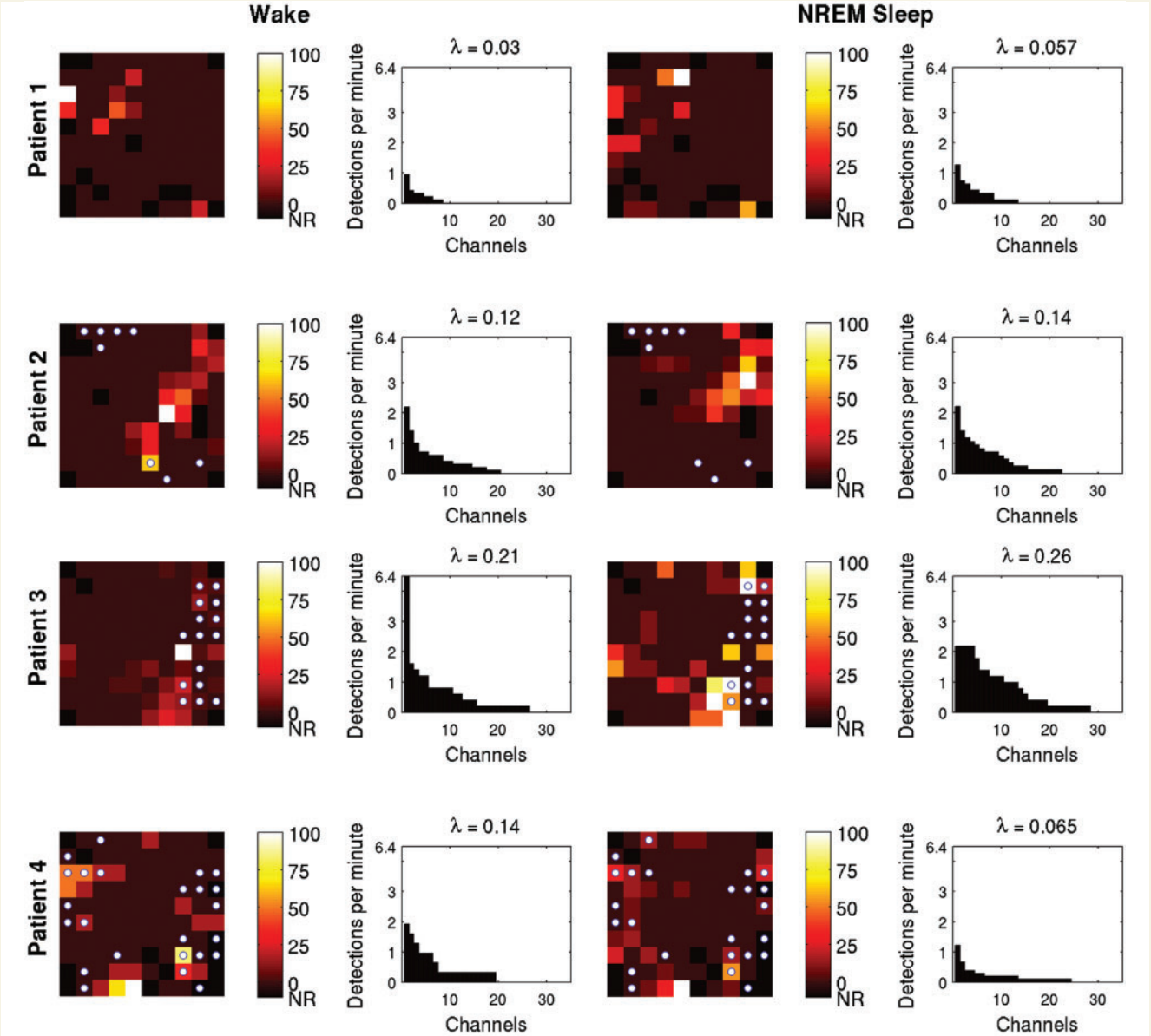

Figure 6 Spatial distribution of HFOs. HFO rate per channel site, per recording sample is depicted in the topographical maps of the MEA, expressed as a percentage of the maximum rate for that sample. Non-recording channels (NR) are shown in black. Microdischarge sites are indicated by the small white circles. The bar plots were obtained by sorting the channels by HFO rate; channels with no HFO detections are excluded. The concentration of HFO generation in a small number of channels is clearly evident, as is the significantly larger distribution of HFO generating sites in Patients 2–4 compared with Patient 1 (Student's *t*-test, $P < 0.05$). Poisson distribution parameters, obtained using maximum likelihood estimation, also were significantly greater in Patients 2–4. Note that the generating regions for HFOs and microdischarges are not co-located, although some overlap is present. Clustering of HFO generating sites near microdischarge sites is particularly evident in Patient 3's data.

often restricted to a single microelectrode and tend to concentrate in a relatively small number of electrode sites.

In contrast to earlier studies, nearly all HFO detections were classified by visual inspection as fast ripples. One possible explanation is that the previous microelectrode studies, both animal and human, have focused almost exclusively on mesial temporal areas while our recordings are all from the neocortex. There may be physiological differences between these areas in the production of HFOs that have yet to be fully explored. For example, Staba *et al*. (2002) found higher rates of ripples contralateral to seizure onset and increased fast ripple rates in ipsilateral structures, while we found no ripples in the one patient in whom the MEA was situated outside the epileptogenic zone. It is also possible that the MEA microelectrodes themselves are more sensitive to high frequency activity; for example, it is known that microwires are more likely to detect high frequencies than depth macroelectrodes, probably due to differences in spatial averaging (Worrell *et al*., 2008). Another possible explanation is that the location of

Table 3 Restricted distribution of HFOs

Patient	Sample	Percentage channels with HFO detections	Percentage channels responsible for 50% of detections	Mean HFO to microdischarge sites distance	Expected distance for uniform distribution
1	Wake	9	2.3	N/A	N/A
	Sleep	15	3.5	N/A	N/A
2	Wake	22	4.4	0.71	1.08
	Sleep	24	4.4	0.83	1.08
3	Wake	27	4.2	0.46	1.20
	Sleep	30	6.3	0.71	1.20
4	Wake	22	4.7	0.19	0.66
	Sleep	28	5.8	0.25	0.66

HFOs are limited to small subregions of the MEA, as indicated both by the percentage of recording channels with any HFO detections and the percentage of channels responsible for half of HFO detections. HFO clusters also tended to be closer than expected to microdischarge sites, an effect that was found to be significant in each case (Wilcoxon signed rank test, $P<0.01$).

our 1 mm long MEA electrodes resulted in selective recording of fast ripples. This might be the case if fast ripples were highly localized to layers 4 or 5, and were therefore often not recorded by microwires positioned to less tightly constrained depths. Similarly, if ripple oscillations are localized to more superficial cortical layers, our sensor may have failed to detect them. Layer specificity of ripples and fast ripples has not been described in human neocortex. However, there is some evidence that at least normally occurring neocortical fast ripples may indeed be layer-specific. Stimulus-induced activity up to 320 Hz in neocortical layers IV and VI has been reported in normal rat barrel cortex (Gibson *et al*., 1999).

We and others have observed a strong correlation of fast ripples with population spikes (Buzsaki *et al*., 1992; Bragin *et al*., 2003, 2007). In contrast, we found ripples to correlate only rarely with multiunit spiking. One possible explanation is that ripples reflect the high frequency inhibitory restraint of pyramidal cells (Prince and Wilder, 1967; Trevelyan *et al*., 2006, 2008). Another proposal is that ripples and fast ripples are generated by electrically-connected pyramidal cells in the absence of synaptic firing, with the network path length determining the rate of the oscillation (Traub and Bibbig, 2000; LeBeau *et al*., 2003). Populations of fast-spiking interneurons firing out of phase in a 'see-saw' pattern have been proposed as a possible mechanism explaining the high oscillation rate of fast ripples (Foffani *et al*., 2007).

High frequency oscillation spatial extent and distribution

The evidence for non-uniform spatial distribution of HFOs is striking. HFOs were detected at 9%–30% of recording sites within the MEA in a Poisson pattern, with half of them seen at 2%–6% of sites. Overall, the area of HFO generation comprised between one-tenth and one-third of the recorded area, or between about 2 and 5 mm^2 out of the 16 mm^2 monitored by the MEA, with the smallest portion in the patient recorded outside the epileptogenic zone. Half of the HFOs were found in <7% of the total recording area, or less than ~1.2 mm^2.

Because contemporaneous HFO detections were not infrequent and were often widely distributed, we found it useful to introduce the term HFOE to describe instances with one or more concurrent detections in different MEA channels. We found that most HFOEs detected in our data (85%) were limited to a single channel, indicating localization to a cortical region of at most 400×400 μm, or approximately the size of a single cortical macrocolumn (Mountcastle, 1997). This finding is consistent with studies of HFOs in hippocampal slice recordings (Buzsaki *et al*., 1992; Bragin *et al*., 2003, 2007) which identified spatial extents of <1 mm^2.

Simultaneous HFO detections have been reported in studies employing microwire bundles, in which the distance between contacts was estimated to be 1 mm (Worrell *et al*., 2008). As the example in Fig. 2b illustrates, large-scale HFOEs were seen to extend over several square millimetres. Moreover, simultaneous transient increases in 100–500 Hz activity were present in several other channels that did not meet criteria for detection, either because signal amplitude was not high enough relative to the baseline activity in that channel to exceed detection threshold, or because there were too few signal peaks outside of the threshold values. This suggests that large-scale HFOEs may occur on a continuum rather than as a binary process, and that binary HFO detection may underestimate the spatial extent of this activation.

While simultaneous detections at two adjacent MEA channels could be due to a HFO arising in a region sampled by both microelectrodes, multiple contemporaneous detections spanning more than two channel sites cannot be explained either in this way or by such mechanisms as volume conduction or reference contamination. First, the majority of detections (85%) were limited to a single channel. Second, large scale events spanning most of the MEA were seen (Fig. 5), an observation incompatible with simple volume conduction from a single source. Third, close examination of the signal in adjacent contacts, such as those illustrated in Fig. 5, reveal differences in morphology, frequency spectra and timing of amplitude peaks that can only be the result of independent sources. These findings are a strong indication that HFOE generation can occur simultaneously across larger cortical regions, as was seen in 12% of HFOEs in this study. Moreover, data from all MEA channels during an HFOE (Fig. 2b) reveals that high frequency activity is increased in many channels that did not

meet criteria for automated detection. We conclude, then, that while most HFOs appear to be highly focal, perhaps limited to a single cortical microdomain, there is a subclass of HFOs that have a large scale component, most commonly seen in association with interictal epileptiform events.

High frequency oscillations and interictal epileptiform events

Large-scale HFOEs were associated with macrodischarges 80% of the time, a rate close to that reported in studies using cortical or depth macroelectrodes (Urrestarazu *et al*., 2007; Worrell *et al*., 2008). This observation points to the phenomenon of large-scale HFOEs as a plausible explanation for the ability of depth macroelectrodes to detect HFOs, an otherwise surprising finding given the limited size of individual HFOs compared with the recording area of macroelectrodes.

Microdischarges are limited to small subregions within the MEA and, as such, probably originate locally (Schevon *et al*., 2008). Macrodischarges, however, represent more widespread epileptiform events and may originate as distant events that then propagate to the MEA (Fig. 3) (Emerson *et al*., 1995; Schevon *et al*., 2008). While, it is clear from both the prior literature and the present study that HFOs occur more frequently within the epileptogenic zone, and that they are prominent in the epileptogenic zone at the onset of seizures (Jirsch *et al*., 2006), our observations of large-scale HFOEs suggest either simultaneous initiation of HFO activity in multiple cortical domains through an as yet undiscovered mechanism, or that the activity constitutes a local response to a neurally propagated triggering epileptiform event.

Despite the lack of association between HFOs and microdischarges in both the spatial and temporal domains, a relationship between the two is possible. The distance between HFO and microdischarge sites was generally less than would be expected based on a uniform distribution. Bragin *et al*. (2000) have hypothesized that during epileptogenesis, tiny 'pathologically interconnected neuron clusters' coalesce to form an epileptogenic network and generate fast ripples (Bragin *et al*., 2000). Consistent with this view, we propose that microdischarges are produced by locally excitable clusters, and that cortical domains near microdischarge sites become primed to produce fast ripples; the latter are most effectively associated with well developed, propagating interictal epileptiform events.

High frequency oscillations as markers of epileptogenic cortex

Multiple studies have shown fast ripples to be more frequent in epileptogenic mesial temporal structures than in the unaffected side; indeed, they may serve as a useful biomarker of epileptogenic cortex (Staba *et al*., 2002; Jacobs *et al*., 2008; Worrell *et al*., 2008). Limited data exist suggesting that the same may be true in neocortical epilepsy syndromes. Although the number of patients recorded is small, with only one recorded outside the epileptogenic zone, the results of our study support this hypothesis. Rates of HFOs, large-scale HFOEs and the number of channels generating HFOs were all higher in Patients 2–4, in whom the MEA was located within the epileptogenic zone, than in Patient 1. The implant site in Patient 1, while included in the subsequent standard anterolateral temporal lobectomy, was presumed not to be epileptogenic due to the absence of interictal epileptiform activity. Microdischarges, another potential marker of epileptogenic cortex, were also absent.

Our findings highlight some of the strengths and limitations of commonly available methods of sampling HFOs. Sparsely distributed microwires may miss the strongest HFO-generating sites, and may be more likely to do so outside of the epileptogenic zone. Macroelectrodes are most likely to detect large-scale HFOEs, which are potentially clinically useful as they appear to be the best predictor of the epileptogenic zone.

References

Bikson M, Fox JE, Jefferys JGR. Neuronal aggregate formation underlies spatiotemporal dynamics of nonsynaptic seizure initiation. J Neurophysiol 2003; 89: 2330–3.

Bragin A, Azizyan A, Almajano J, Wilson CL, Engel J. Analysis of chronic seizure onsets after intrahippocampal kainic acid injection in freely moving rats. Epilepsia 2005; 46: 1592–8.

Bragin A, Engel J, Wilson CL, Fried I, Buzsaki G. High-frequency oscillations in human brain. Hippocampus 1999; 9: 137–42.

Bragin A, Mody I, Wilson CL, Engel J. Local generation of fast ripples in epileptic brain. J Neurosci 2002; 22: 2012–21.

Bragin A, Wilson CL, Engel J. Spatial stability over time of brain areas generating fast ripples in the epileptic rat. Epilepsia 2003; 44: 1233–7.

Bragin A, Wilson CL, Engel J. Voltage depth profiles of high-frequency oscillations after kainic acid-induced status epilepticus. Epilepsia 2007; 48: 35–40.

Bragin A, Wilson CL, Engel J Jr. Chronic epileptogenesis requires development of a network of pathologically interconnected neuron clusters: a hypothesis. Epilepsia 2000; 41 (Suppl 6): S144–52.

Buzsaki G, Horvath Z, Urioste R, Hetke J, Wise K. High-frequency network oscillation in the Hippocampus. Science 1992; 256: 1025–27.

Cash SS, Halgren E, Dehghani N, Rossetti AO, Thesen T, Wang C, et al. The human K-complex represents an isolated cortical down-state. Science 2009; 324: 1084–7.

Emerson RG, Turner CA, Pedley TA, Walczak TS, Forgione M. Propagation patterns of temporal spikes. Electroencephal Clin Neurophysiol 1995; 94: 338–48.

Foffani G, Uzcategui YG, Gal B, Menendez de la Prida L. Reduced spike-timing reliability correlates with the emergence of fast ripples in the rat epileptic hippocampus. Neuron 2007; 55: 930–41.

Gibson JR, Beierlein M, Connors BW. Two networks of electrically coupled inhibitory neurons in neocortex. Nature 1999; 402: 75–9.

Haueisen J, Schack B, Meier T, Curio G, Okada Y. Multiplicity in the high-frequency signals during the short-latency somatosensory evoked cortical activity in humans. Clin Neurophysiol 2001; 112: 1316–25.

Hochberg LR, Serruya MD, Friehs GM, Mukand JA, Saleh M, Caplan AH, et al. Neuronal ensemble control of prosthetic devices by a human with tetraplegia. Nature 2006; 442: 164–71.

House PA, MacDonald JD, Tresco PA, Normann RA. Acute microelectrode array implantation into human neocortex: preliminary technique and histological considerations. Neurosurg Focus 2006; 20: 1–4.

Jacobs J, Levan P, Chander R, Hall J, Dubeau F, Gotman J. Interictal high-frequency oscillations (80-500 Hz) are an indicator of seizure

onset areas independent of spikes in the human epileptic brain. Epilepsia 2008; 49: 1893–907.

Jirsch JD, Urrestarazu E, LeVan P, Olivier A, Dubeau F, Gotman J. High-frequency oscillations during human focal seizures. Brain 2006; 129: 1593–608.

LeBeau FEN, Traub RD, Monyer H, Whittington MA, Buhl EH. The role of electrical signaling via gap junctions in the generation of fast network oscillations. Brain Res Bull 2003; 62: 3–13.

Mountcastle VB. The columnar organization of the neocortex. Brain 1997; 120: 701–22.

Niedermeyer E, Lopes da Silva F. Electroencephalography: basic principles, clinical applications, and related fields. Baltimore, MD: Lippincott Williams & Wilkins; 1999.

Prince DA, Wilder BJ. Control mechanisms in cortical epileptogenic foci. ''Surround'' inhibition. Arch Neurol 1967; 16: 194–202.

Rosenow F, Luders H. Presurgical evaluation of epilepsy. Brain 2001; 124: 1683–700.

Rousche PJ, Normann RA. Chronic recording capability of the Utah Intracortical Electrode Array in cat sensory cortex. J Neurosci Meth 1998; 82: 1–15.

Schevon CA, Ng SK, Cappell J, Goodman RR, McKhann G, Waziri A, et al. Microphysiology of Epileptiform Activity in Human Neocortex. J Clin Neurophysiol 2008; 25: 321–30.

Schroeder CE, Steinschneider M, Javitt DC, Tenke CE, Givre SJ, Mehta AD, et al. Localization of ERP generators and identification of underlying neural processes. Electroencephalogr Clin Neurophysiol Suppl 1995; 44: 55–75.

Schroeder CE, Tenke CE, Givre SJ. Subcortical contributions to the surface-recorded flash-VEP in the awake macaque. Electroencephalogr Clin Neurophysiol 1992; 84: 219–31.

Staba RJ, Wilson CL, Bragin A, Fried I, Engel J Jr. Quantitative analysis of high-frequency oscillations (80-500 Hz) recorded in human epileptic hippocampus and entorhinal cortex. J Neurophysiol 2002; 88: 1743–52.

Steinschneider M, Tenke CE, Schroeder CE. Cellular generators of the cortical auditory evoked potential initial component. Electroencephalogr Clin Neurophysiol 1992; 84: 196–200.

Suner S, Fellows MR, Vargas-Irwin C, Nakata GK, Donoghue JP. Reliability of signals from a chronically implanted, silicon-based electrode array in non-human primate primary motor cortex. IEEE Trans Neural Syst Rehabil Eng 2005; 13: 524–41.

Traub RD, Bibbig A. A model of high-frequency ripples in the hippocampus based on synaptic coupling plus axon-axon gap junctions between pyramidal neurons. J Neurosci 2000; 20: 2086–93.

Trevelyan AJ. Intrinsic cortical mechanisms which oppose epileptiform activity: Implications for seizure prediction. In: Schelter B, Schulze-Bonhage A, Timmer J, editors. Seizure prediction in epilepsy – from basic mechanisms to clinical applications. Berlin: Wiley-VCH; 2008.

Trevelyan AJ, Sussillo D, Watson BO, Yuste R. Modular propagation of epileptiform activity: Evidence for an inhibitory veto in neocortex. J Neurosci 2006; 26: 12447–55.

Ulbert I, Heit G, Madsen J, Karmos G, Halgren E. Laminar analysis of human neocortical interictal spike generation and propagation: current source density and multiunit analysis in vivo. Epilepsia 2004a; 45: 48–56.

Ulbert I, Magloczky Z, Eross L, Czirjak S, Vajda J, Bognar L, et al. In vivo laminar electrophysiology co-registered with histology in the hippocampus of patients with temporal lobe epilepsy. Exp Neurol 2004b; 187: 310–18.

Urrestarazu E, Chander R, Dubeau F, Gotman J. Interictal high-frequency oscillations (100-500 Hz) in the intracerebral EEG of epileptic patients. Brain 2007; 130: 2354–66.

Wang C, Ulbert I, Schomer DL, Marinkovic K, Halgren E. Responses of human anterior cingulate cortex microdomains to error detection, conflict monitoring, stimulus-response mapping, familiarity, and orienting. J Neurosci 2005; 25: 604–13.

Waziri A, Schevon C, Cappell J, Emerson R, McKhann G, Goodman R. Initial surgical experience with a dense cortical microarray in epileptic patients undergoing craniotomy for subdural electrode implantation. Neurosurgery 2009; 64: 540–5; discussion 545.

Worrell GA, Gardner AB, Stead SM, Hu S, Goerss S, Cascino GJ, et al. High-frequency oscillations in human temporal lobe: simultaneous microwire and clinical macroelectrode recordings. Brain 2008; 131: 928–37.